Pathways of the Extremely Reactive Iron(IV)-oxido complexes with Tetradentate Bispidine Ligands

Mahmud Abu-Odeh,[a] Katharina Bleher+,[a] Neethinathan Johnee Britto,[b] Peter Comba,*[a, c] Michael Gast,[a] Madhavan Jaccob,[b] Marion Kerscher,[a] Saskia Krieg+,[a] and Marius Kurth[a]

Abstract: The nonheme iron(IV)-oxido complex *trans*-N3-[(L^1)Fe^{IV}=O(Cl)]$^+$, where L^1 is a derivative of the tetradentate bispidine 2,4-di(pyridine-2-yl)-3,7-diazabicyclo[3.3.1]nonane-1-one, is known to have an $S=1$ electronic ground state and to be an extremely reactive oxidant for oxygen atom transfer (OAT) and hydrogen atom abstraction (HAA) processes. Here we show that, in spite of this ferryl oxidant having the "wrong" spin ground state, it is the most reactive nonheme iron model system known so far and of a similar order of reactivity as nonheme iron enzymes (C–H abstraction of cyclohexane, −90 °C (propionitrile), $t_{1/2}=3.5$ sec). Discussed are spectroscopic and kinetic data, supported by a DFT-based theoretical analysis, which indicate that substrate oxidation is significantly faster than self-decay processes due to an intramolecular demethylation pathway and formation of an oxido-bridged diiron(III) intermediate. It is also shown that the iron(III)-chlorido-hydroxido/cyclohexyl radical intermediate, resulting from C–H abstraction, selectively produces chlorocyclohexane in a rebound process. However, the lifetime of the intermediate is so long that other reaction channels (known as cage escape) become important, and much of the C–H abstraction therefore is unproductive. In bulk reactions at ambient temperature and at longer time scales, there is formation of significant amounts of oxidation product – selectively of chlorocyclohexane – and it is shown that this originates from oxidation of the oxido-bridged diiron (III) resting state.

Introduction

High-valent iron-oxygen species have attracted much interest after the discovery and thorough characterization of non-heme iron-oxido enzymes and model systems in the early 2000s.[1–3] Of particular interest are the diverse reactivities and mechanistic patterns, that is, electrophilic as well as nucleophilic, hydrogen atom abstraction (HAA) and oxygen atom transfer (OAT), derived from numerous mechanistic studies that have led to a thorough understanding of the structural and emerging electronic and spectroscopic properties of enzymes and model systems and their correlation with reactivities, and consequently also have initiated applications in organic synthesis and environmental sciences.[4–8] Important and still disputed aspects are related to the fact that all enzymes have a high-spin ($S=2$) electronic ground state, while many model systems are intermediate-spin ($S=1$): on one hand, this relates to missing data and the often underestimated importance of the driving force (i.e. the $Fe^{IV/III}$-oxido redox potential, an experimental parameter that is very difficult to access accurately),[9–12] and on the other hand it is associated with the two-state-reactivity concept (TSR) and the fact that the spin state of the ferryl complex might be less important than the energy gap to the high-spin state.[13–16]

Bispidine-iron(IV)-oxido complexes have been studied extensively.[17–26] An interesting feature is the rigidity of the bispidine scaffold that is too large for Fe^{IV}=O and therefore enforces high redox potentials of the ferryl species.[27] A range of easily accessible ligands with differing denticity and donor sets allows to fine-tune the reactivities of the bispidine-ferryl oxidants.[28,29] Of particular interest is the complex with the simplest tetradentate bispidine (L^1 in Scheme 1): after earlier indications that the corresponding chlorido-ferryl complex is high-spin ($S=2$), it recently has been shown to have an intermediate-spin ($S=1$) electronic ground state and,[30] with cyclohexane as substrate, [(L^1)Fe^{IV}=O(Cl)]$^+$ (see Scheme 1) selectively leads to chlorocyclohexane and is the most powerful and fastest known low molecular weight ferryl oxidant:[21,31] the chlorido-oxido-complex [(L^1)Fe^{IV}=O(Cl)]$^+$ decays at −90 °C with

[a] M. Abu-Odeh, Dr. K. Bleher,+ Prof. Dr. P. Comba, Dr. M. Gast, Dr. M. Kerscher, Dr. S. Krieg,+ M. Kurth
Anorganisch-Chemisches Institut
Universität Heidelberg
INF 270, 69120 Heidelberg (Germany)
E-mail: peter.comba@aci.uni-heidelberg.de

[b] N. Johnee Britto, Prof. M. Jaccob
Department of Chemistry
Loyola College
Chennai 600034 (India)

[c] Prof. Dr. P. Comba
Interdisziplinäres Zentrum für Wissenschaftliches Rechnen (IWR)
Mathematikon
Im Neuenheimer Feld 205, 69120 Heidelberg (Germany)

[+] This work is part of the PhD theses of Katharina Bleher and Saskia Krieg.

Supporting information for this article is available on the WWW under https://doi.org/10.1002/chem.202101045

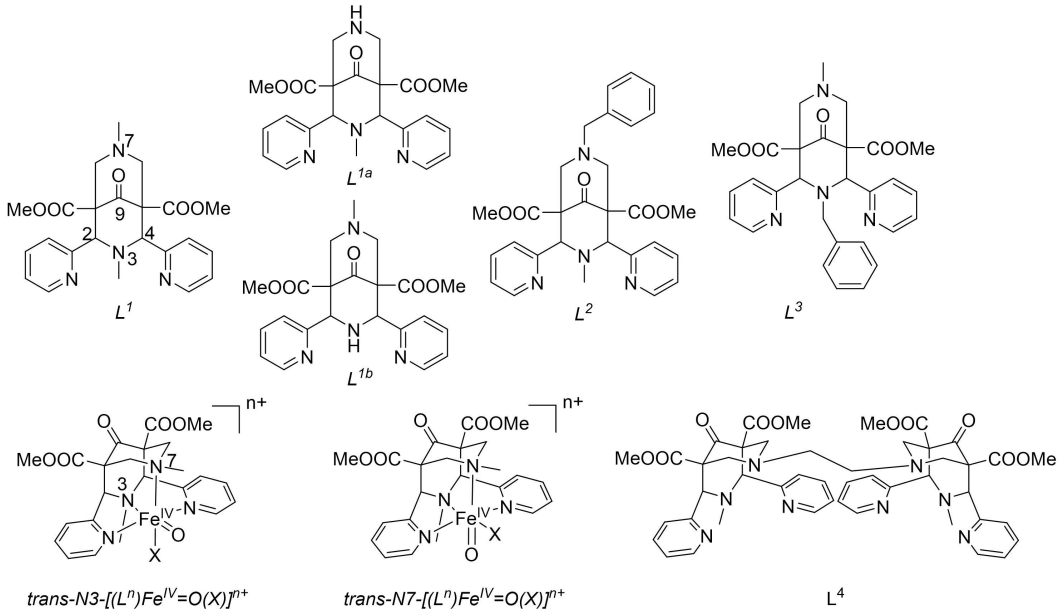

Scheme 1. Ligands and complexes discussed in this manuscript; X = Cl^- or MeCN (the specification "*trans*-N3" will generally be omitted for simplicity since *trans*-N3-$[(L^n)Fe^{IV}=O(X)]^{n+}$ is the relevant species in the context of most discussions below).

a half-life of minutes, only approx. 25 times slower than with cyclohexane as substrate.[32–37]

Here, we describe a thorough analysis of the various pathways of the self-decay reaction by tandem mass spectrometry, cryo-stopped-flow kinetics, a mechanistic DFT study, and the product analysis of bulk reactions with the ferryl complexes of L^1 and the isomeric pair of the ligand derivatives L^2 and L^3.

Results and Discussion

Mass spectrometry and crystallography

HR-ESI MS (high resolution electrospray ionization mass spectrometry) was used to characterize the products formed in situ by oxido-transfer reactions to the $[(L^1)Fe^{II}Cl_2]$ precursor with the soluble iodosylbenzene reagent ^{s}PhIO (^{s}PhIO = 1-(tert-butylsulfonyl)-2-iodosylbenzene) in acetonitrile (MeCN).[38] At relatively low concentration of oxidant (Figure 1; see Supporting Information for additional spectra with other oxidant concentrations and for the simulation of the isotope patterns of the major signals, Figures S1–S4) unreacted $[(L^1)Fe^{II}Cl_2]$ precursor is a prominent species (*m/z* $[(L^1)Fe^{II}Cl]^+$ calcd. 529.0936, obsd. 529.0938), and the other major signal is assigned to the μ-oxido-bridged diiron(III) decay product $[Cl(L^1)Fe^{III}\text{-}O\text{-}Fe^{III}(L^1)Cl]^{2+}$ (*m/z* $[Cl(L^1)Fe^{III}\text{-}O\text{-}Fe^{III}(L^1)Cl]^{2+}$ calcd. 537.0910, obsd. 537.0914). These mono-oxido-bridged diiron(III) complexes usually are fairly unreactive. However, depending on the ligand sphere, diiron(III) complexes can be oxidized to higher valent species with high oxidation power (e.g. model systems for the methane mono-oxygenase active site).[33,39–41] The preferential formation of the dinuclear complex at low oxidant concentrations suggests that its putative precursor, the iron(IV)-oxido complex

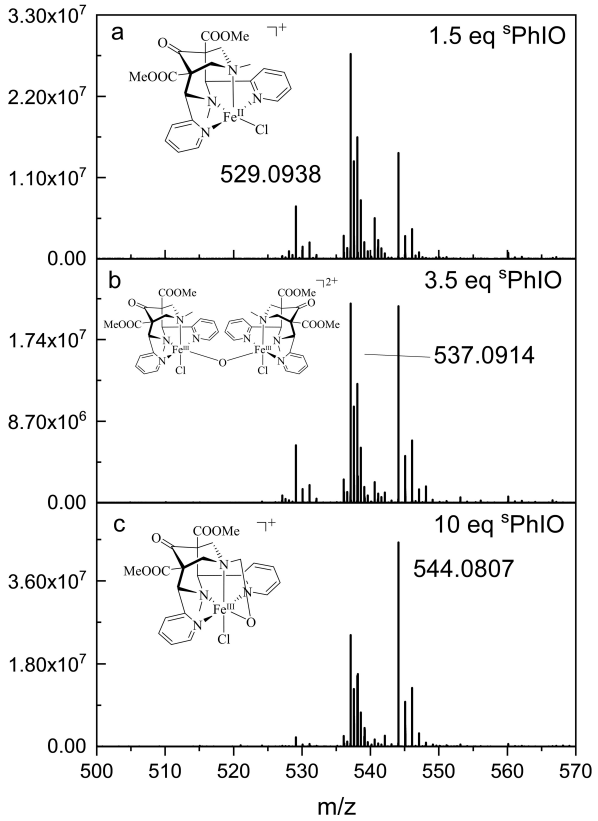

Figure 1. ESI-MS spectra of in situ reactions of $[(L^1)Fe^{II}Cl_2]$ (10 μM in MeCN) with ^{s}PhIO (a: 1.5 eq, b: 3.5 eq, c: 10 equiv. ^{s}PhIO) at 298 K (spectra were recorded after 60 min reaction time). See Supporting Information for the general procedure and simulated isotopic patterns (Figures S1 – S3).

$[(L^1)Fe^{IV}=O(Cl)]^+$ is very reactive and that, therefore, the formation of the diiron(III) decay product by a second order reaction from the ferryl complex $[(L^1)Fe^{IV}=O(Cl)]^+$ and unreacted iron(II) precursor is very fast. It emerges that the only chance to trap $[(L^1)Fe^{IV}=O(Cl)]^+$ is to use an excess of the ^{s}PhIO oxidant in order to significantly accelerate the formation reaction. Indeed, at higher concentrations of ^{s}PhIO, the signal at $m/z=544.0807$ becomes the major signal in the ESI-MS spectra (see Figure 1, m/z $[(L^1\text{-H})Fe(O)(Cl)]^+$ calcd. 544.0807, obsd. 544.0807). The assumed structure of this mechanistically important species, i.e. $[(L^1\text{-H})Fe(O)(Cl)]^+$, is included in Figure 1c: we suggest that it results from intramolecular C–H abstraction by the ferryl complex at the methyl group at N7, followed by a rebound step and proton loss. Therefore, formally this species is an uncharged Fe^{II} complex, which however is observed as a monocation. One-electron oxidation of neutral species in positive-mode ESI-MS is not uncommon and has been observed before in ferryl oxidation chemistry.[42,43]

An oxido-bridged diiron(III) complex of the N7-demethylated bispidine L^{1a} and coordinated bromide ions to complete the coordination spheres of both iron(III) centers, $[Br(L^{1a})Fe^{III}\text{-O-}Fe^{III}(L^{1a})Br]Br_2\cdot 4MeCN$, could be crystallized, and a plot of the molecular cation is shown in Figure 2 (see Supporting Information for crystallographic details). The complex has the coordinated Br^- donors exo to each other and the structure is centro-symmetric with respect to the bridging oxido group. The C9 ketone groups are hydrolyzed, as is often observed with metal complexes of L^1,[28,44] and the structural parameters of the coordination polyhedra are as expected (see Supporting Information which, for comparison, also shows crystal structural data of the iron(II) precursors with coordinated Cl^- and Br^-, as well as of the diiron(II) complex with a similar dinucleating bispidine ligand (L^4), Figures S28, S29, Table S11).[11,45]

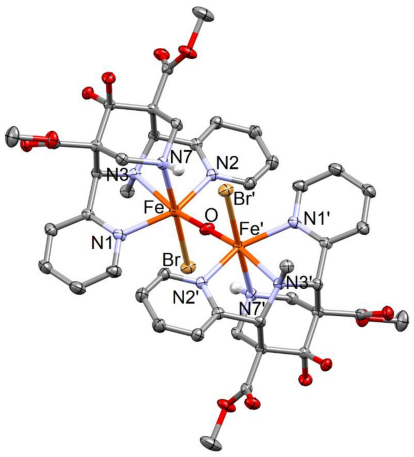

Figure 2. ORTEP plot of the μ-oxido bridged diiron(III) complex $[Br(L^{1a})Fe^{III}\text{-O-}Fe^{III}(L^{1a})Br]Br_2\cdot 4MeCN$. Ellipsoids are shown at the 50% probability level; co-crystallized solvent molecules, counter ions, and hydrogen atoms (except protons at N7 and N7′) are omitted for clarity. Bond lengths: Fe–N1: 2.128(3) Å, Fe–N2: 2.127(3) Å, Fe–N3: 2.239(2) Å, Fe–N7: 2.231(3) Å, Fe–Br: 2.5184(5) Å, Fe–O: 1.7795(4) Å.

To further investigate the identity of $[(L^1\text{-H})Fe^{III}(O)(Cl)]^+$, we performed tandem MS (see Figure 3, see Supporting Information, Figures S3 and S4, for additional spectra and simulations of the isotope patterns) in a voltage range of 5–10 V. The isolated $[(L^1\text{-H})Fe^{III}(O)(Cl)]^+$ intermediate decays with CH_2O release to the demethylated iron(III) complex $[(L^{1a}\text{-H})Fe^{III}(Cl)]^+$ (m/z $[(L^{1a}\text{-H})Fe^{III}(Cl)]^+$ calcd. 514.0706, obsd. 514.0708, see Scheme 1 for the structure of L^{1a}), where N7 is deprotonated. There are few other examples of ligand-centered N-demethylation processes of oxygen adducts of transition metal complexes,[43] and N7-demethylation of the coordinated bispidine L^1 to L^{1a} has been observed before in $L^1\text{-}Co^{II}/H_2O_2$ chemistry.[46] N-demethylation was also observed with the less reactive MeCN-based analogue $[(L^1)Fe^{IV}=O(MeCN)]^{2+}$ (see Figure 3c,d; m/z $[(L^1\text{-H})Fe^{III}(O)(MeO^-)]^{2+}$: calcd. 540.1302, obsd. 540.1303, [m/z $(L^{1a}\text{-H})Fe^{III}(MeO^-)]^+$: calcd. 510.1202, obsd. 510.1198, see also Supporting Information, Figure S5; note, that in the ESI-MS the co-ligand MeCN is substituted to the negatively charged MeO^- to reduce charge density).[47]

To probe, whether the demethylation process is an intra- or an intermolecular reaction, the two isomeric mono-*N*-benzylated ligands L^2 and L^3 were prepared, and their iron(II) precursors were oxidized *in situ* with ^{s}PhIO to *trans*-N3-$[(L^2)Fe^{IV}=O(Cl)]^+$ and *trans*-N3-$[(L^3)Fe^{IV}=O(Cl)]^+$ and also studied by tandem MS (see Figure 4). The orientation of the oxido-group in the two isomers is derived from density functional theory (DFT), which indicates that the *trans*-N3-$[(L^n)Fe^{IV}=O(Cl)]^+$ (n = 1,2,3) geometry generally is more stable than the corresponding *trans*-N7 isomers (see Scheme 1).[12,19,48] Therefore, in an intermolecular process, both isomers, *trans*-N3-$[(L^2)Fe^{IV}=O(Cl)]^+$ and *trans*-N7-$[(L^3)Fe^{IV}=O(Cl)]^+$ should lead to a fragmentation of the $[(L^n\text{-H})Fe^{III}(O)(Cl)]^+$ (n = 2,3) species with similar ratios of PhCHO (benzaldehyde) and CH_2O (formaldehyde) release and formation of $[(L^{1a}\text{-H})Fe^{III}(Cl)]^+$ or $[(L^{1b}\text{-H})Fe^{III}(Cl)]^+$ and the corresponding benzylated derivatives. In contrast, an intramolecular C–H activation by the oxido-group should only with *trans*-N3-$[(L^2)Fe^{IV}=O(Cl)]^+$ produce PhCHO, while *trans*-N3-$[(L^3)Fe^{IV}=O(Cl)]^+$ should release CH_2O and yield the N3-benzylated iron(III) product. From Figure 4c it emerges that the N7-benzylated ferryl complex (L^2) preferentially fragments with benzaldehyde release, while the isomeric N3-benzylated isomer (L^3) in Figure 4a preferentially fragments with formaldehyde release (see Supporting Information for more details, also including the formation of phenol derivatives of the benzylated ligands, Scheme S1 and Figures S7 and S9).

The conclusion from mass spectrometry is that, under the conditions of the MS experiments,[38] the very reactive ferryl complex $[(L^1)Fe^{IV}=O(Cl)]^+$ and its analogues with L^2 and L^3 decay via two major pathways: (i) reaction of the ferryl complex with excess iron(II) precursor to a μ-oxido-bridged diiron(III) species, i.e. a process with second order kinetics that can be partially suppressed by increasing the second order rate of the ferryl complex formation reaction with an excess of the ^{s}PhIO oxidant, and (ii) the ferryl-initiated demethylation, an intramolecular process with first order kinetics, see Scheme 2. Note that the product of the dealkylation process always is an oxygenated species (rebound to the Fe^{III}-OH subunit, i.e.

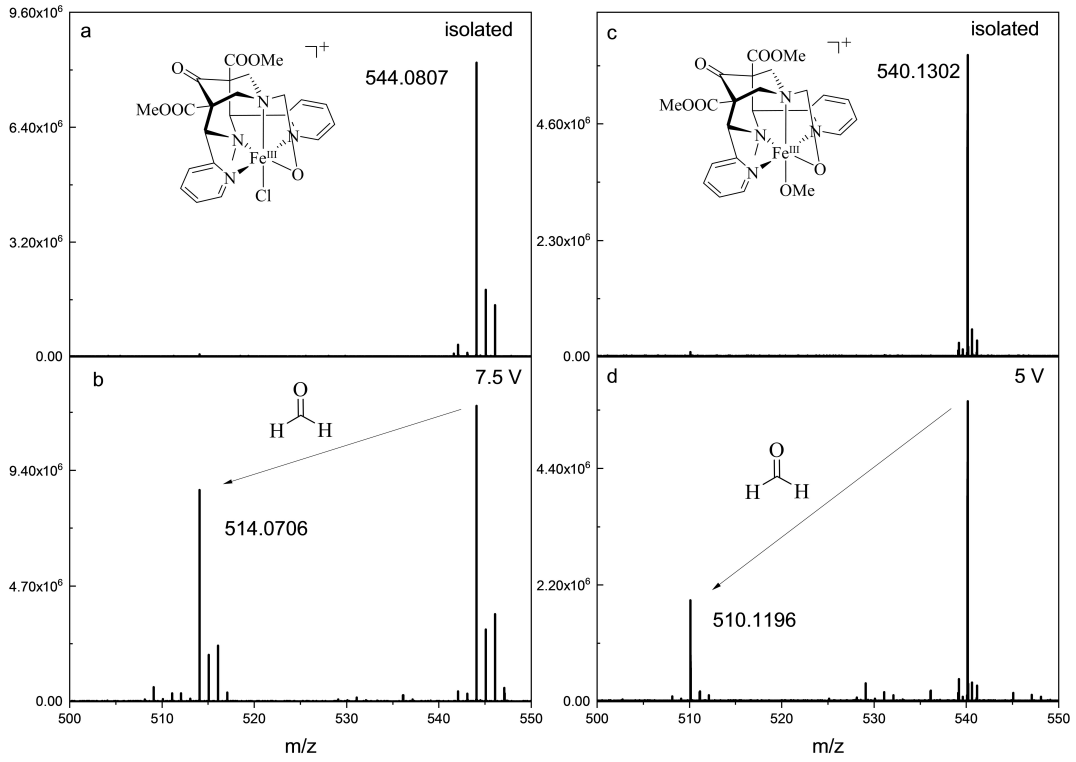

Figure 3. Tandem-MS of *in situ* reactions of $[(L^1)Fe^{II}Cl_2]$ (a: isolated peak, b: 7.5 V fragmentation voltage) and $[(L^1)Fe^{II}(MeCN)_2]^{2+}$ (c: isolated peak, 5 V fragmentation voltage) (10 μM in MeCN) with ^{s}PhIO (35 μM) at 298 K (spectra were recorded after 60 min reaction time). See Supporting Information for general procedures and other voltages used (Figure S5).

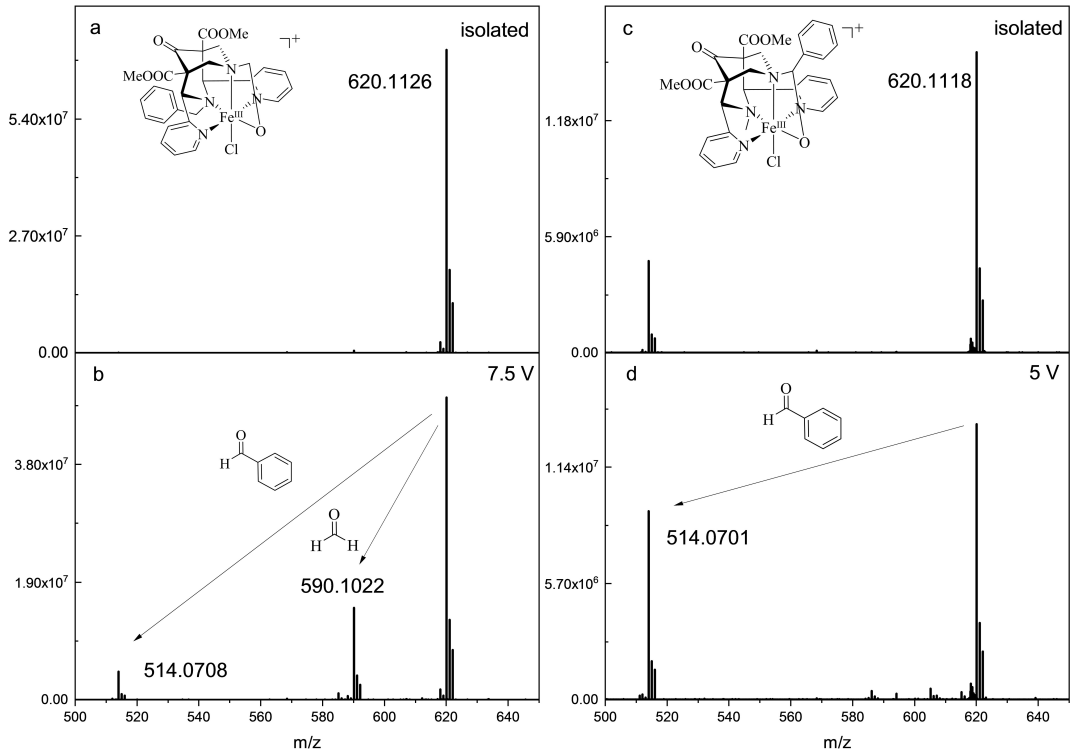

Figure 4. Tandem-MS of *in situ* reactions of $[(L^2)Fe^{II}Cl_2]$ (10 μM in MeCN): c, isolated peak, d, 5 V fragmentation voltage, and of $[(L^3)Fe^{II}Cl_2]$ (10 μM in MeCN): a, isolated peak, b, 7.5 V fragmentation voltage, with ^{s}PhIO (35 μM in MeCN) at 298 K (spectra were recorded after 60 min reaction time). For general procedure and other voltages see Supporting Information (Figures S7 and S9).

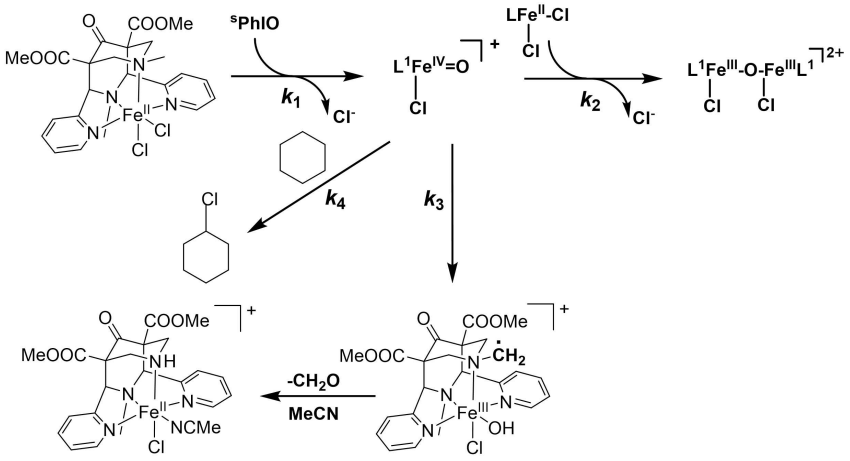

Scheme 2. Formation of $[(L^1)Fe^{IV}=O(Cl)]^+$ (k_1), its decay to the oxido-bridged diiron(III) complex (k_2), decay by $Fe^{IV}=O$ based C–H activation, leading to demethylation (k_3), and reaction with a substrate (cyclohexane oxidation, k_4).

formaldehyde with L^1 and L^3, and benzaldehyde with L^2). Included in addition to these self-decay reactions with rate constants k_2 and k_3, respectively, is the reaction of the ferryl oxidant with substrate [cyclohexane, rate constant k_4] that will be discussed in the next section. An important question that will be further discussed below relates to the relative stability and reactivity (the life-time) of the ferryl complex $[(L^1)Fe^{IV}=O(Cl)]^+$.

Kinetics

Cryo-stopped-flow (dry MeCN or EtCN, 180–240 K, Ar) was used to study the formation and decay kinetics of $[(L^1)Fe^{IV}=O(Cl)]^+$ (rates k_1, k_2, k_3, k_4 in Scheme 2).[38,49] A major problem of the kinetic study is the exceedingly high reactivity of $[(L^1)Fe^{IV}=O(Cl)]^+$, i.e. the ferryl species can only be prepared in situ and with an excess of oxidant (see Scheme 2 and Figure 5). For this reason, it is virtually impossible to study true stoichiometric processes and the various pathways separately. Therefore, and due to the relatively unstructured UV-vis-NIR data and complex kinetic network, attempts for global fitting of the time-dependent spectroscopic data failed (see also Supporting Information).

Formation of $[(L^1)Fe^{IV}=O(Cl)]^+$ with an excess of ^{s}PhIO could be measured by the decay of a charge transfer transition (CT) of $[(L^1)Fe^{II}Cl_2]$ at 460 nm and therefore at low complex concentration (75 μM) with a large excess of ^{s}PhIO (10 eq). Most other kinetic experiments were done with $[(L^1)Fe^{II}Cl_2]$ concentrations in the millimolar range and with a moderate excess of ^{s}PhIO (max. solubility in MeCN of approx. 4 mM; time-dependence of the dd transition of $Fe^{IV}=O$ at around 850 nm). All reported kinetic data are averages of at least 3 experiments and are reported with the corresponding standard deviations. Electronic spectra of the relevant ferryl complexes are shown in Figure 5c and Figure 6a (parameters are tabulated in the Supporting Information, Table S10).

An overview of the time-dependent change for the reaction of $[(L^1)Fe^{II}Cl_2]$ (2 mM) with ^{s}PhIO (2 eq) in EtCN at 183 K is given for the dd transition of the iron(IV)-oxido species at 850 nm in Figure 5b, and the time dependence of the spectra of the decay is shown in Figure 5a. The reaction is best described in three stages: first, the fast oxidation of the iron(II) complex to the ferryl species within 4 s, then decay of the $Fe^{IV}=O$ complex over approx. 70 s by a higher order reaction, whereby an isosbestic point at 570 nm is observed, and finally a slower exponential decay (see Supporting Information for the time-dependent changes of the absorption spectra for the three phases, Figure S14).

The first reaction phase – fast formation of the ferryl complex – was also studied at a CT band of $[(L^1)Fe^{II}Cl_2]$ (460 nm) and therefore at very low concentration of the iron(II) precursor (75 μM) and a relatively large excess of ^{s}PhIO (10 eq; see Supporting Information for the kinetic traces, Figure S16). The kinetics were fitted as a second order process and the resulting rate constant is $k_1=(1.48\pm0.06)\ 10^3\ M^{-1}s^{-1}$ (the pseudo-first-order rate constant, estimated from the traces in the Supporting Information, is $k_1^{obs}=1.2\ s^{-1}$).

From time-traces of the decay process of $[(L^1)Fe^{IV}=O(Cl)]^+$ at various temperatures and with various ^{s}PhIO concentrations (Figure 5b and Supporting Information) it emerges that there are two pathways with differing kinetic parameters, and this is in agreement with the MS data (see above) that suggest a second-order decay to an oxido-bridged diiron(III) complex, competing with the first-order demethylation reaction of the coordinated ligand. The kinetic analysis indicates that the second decay phase (dominating the time-traces after approx. 100 sec in the trace in Figure 5b) is the demethylation reaction, while the first decay phase is dominated by the formation of the oxido-bridged diiron(III) complex. On the basis of the current experimental data, we can only provide indirect kinetic parameters for the first phase of the decay process, i.e. the formation of $[Cl(L^1)Fe^{III}\text{-}O\text{-}Fe^{III}(L^1)Cl]^{2+}$: A comparable dinuclear complex was synthesized with ligand L^4 that has an ethyl bridge

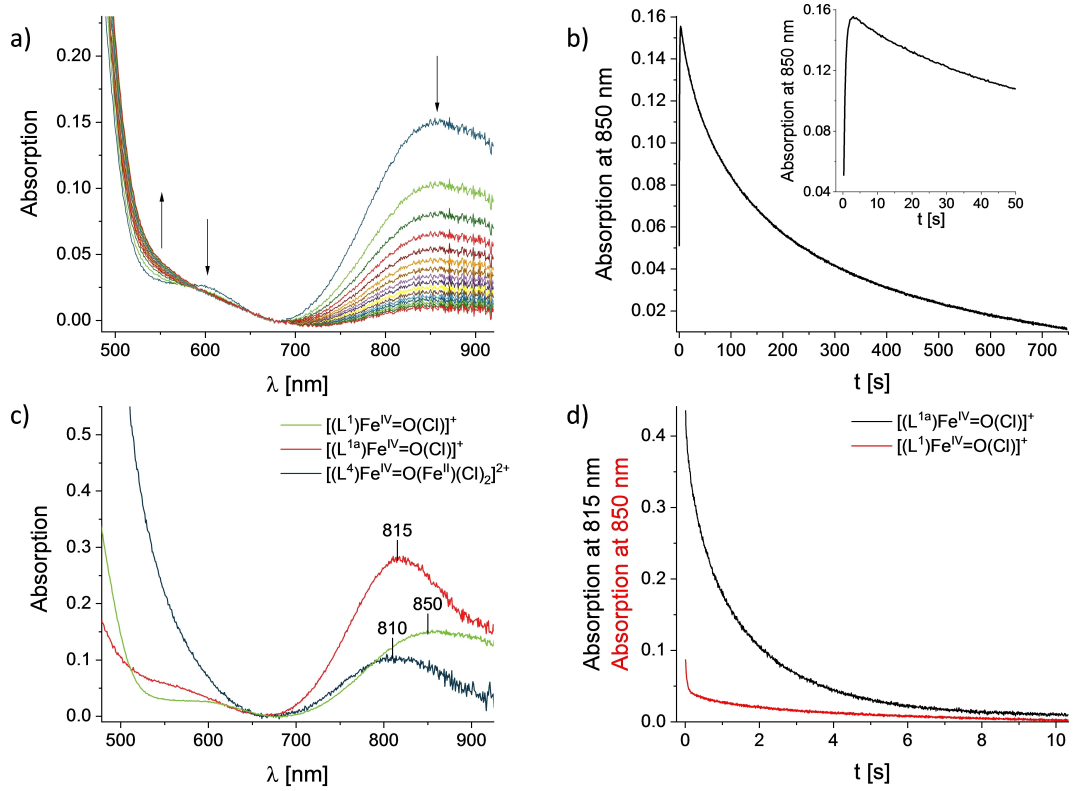

Figure 5. a) Time-dependent spectra of the decay of $[(L^1)Fe^{IV}=O(Cl)]^+$ in EtCN at 183 K. Time between each spectrum is 50 s. b) Time-dependent increase and decay of the absorption band at 850 nm of $[(L^1)Fe^{IV}=O(Cl)]^+$ in EtCN at 183 K following oxidation of the iron(II)precursor (2 mM) with ^{s}PhIO (2 eq) c) Absorption spectra of $[(L^1)Fe^{IV}=O(Cl)]^+$ (green), $[(L^{1a})Fe^{IV}=O(Cl)]^+$ (red) and $[(L^4)Fe^{IV}=O(Fe^{II})(Cl)_2]^{2+}$ (black) in MeCN at 238 K (2 mM Fe^{II} precursor). d) Comparison of the time-dependent decay of the iron(IV)-oxido absorption band of $[(L^1)Fe^{IV}=O(Cl)]^+$ at 850 nm (red) and $[(L^{1a})Fe^{IV}=O(Cl)]^+$ at 815 nm (black) in MeCN at 238 K.

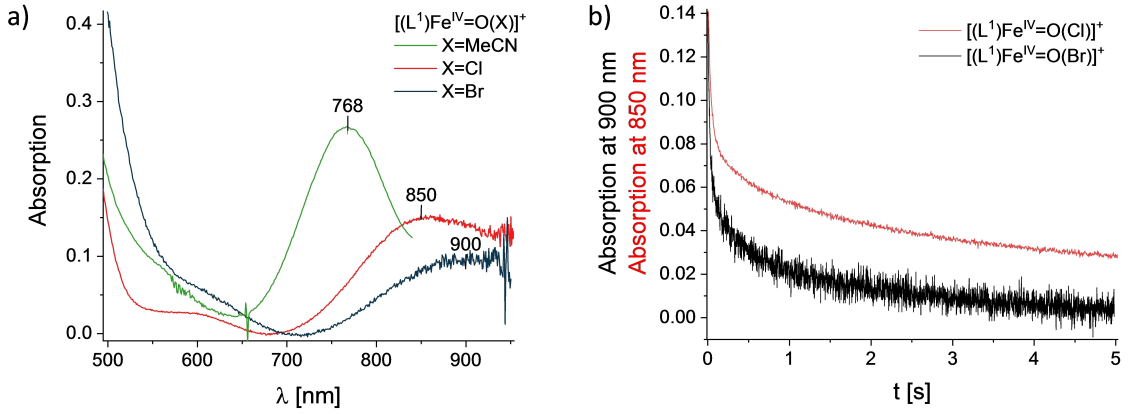

Figure 6. a) Absorption spectra of $[(L^1)Fe^{IV}=O(MeCN)]^{2+}$ (green), $[(L^1)Fe^{IV}=O(Cl)]^+$ (red) $[(L^1)Fe^{IV}=O(Br)]^+$ (black) in MeCN at 238 K. b) Comparison of the time-dependent decay of the iron(IV)-oxido absorption band of $[(L^1)Fe^{IV}=O(Cl)]^+$ at 850 nm (red) and $[(L^1)Fe^{IV}=O(Br)]^+$ at 900 nm (black) in MeCN at 238 K after oxidation of the iron(II) precursor (2 mM) with ^{s}PhIO (2 eq).

between the N7 atoms of two L^1-derived bispidine pockets. The oxidation of the precursor $[(L^4)Fe^{II}_2Cl_4]$ (2 mM) with ^{s}PhIO (5 eq) results in an oxidation product with an absorption band at 810 nm, assigned to the iron(IV)-oxido species (see Figure 5c for the UV-vis-NIR spectrum). The decay of the 810 nm transition was fitted with first order kinetics, and the mass spectrum confirms the oxido-bridged diiron(III) complex as the single product (see Supporting Information, Figure S10). The rate constant $k_{dinucl.}=(0.13\pm0.01)\ s^{-1}$ can be used as an indication of the order of magnitude of the formation rate of a dinuclear complex. At the relatively low concentration of $[(L^1)Fe^{IV}=O(Cl)]^+$ (significantly lower than 1 mM) the decay rate of the ferryl intermediate leading to the formation of the oxido-bridged diiron(III) complex k_2 must be significantly slower.

Fitting of the kinetic data of the second decay phase to first-order kinetics (see Figure 5d) leads to $k_3 = (5.82 \pm 0.59) \cdot 10^{-3}\ s^{-1}$. This is also supported by kinetics followed at 360 nm with 40 μM Fe^{II} precursor (see Supporting Information, Figure S18). Temperature-dependent kinetics (180-225 K) have allowed to determine the activation enthalpy $\Delta H^{\neq} = (41.9 \pm 1.2)\ kJ\,mol^{-1}$ and the activation entropy $\Delta S^{\neq} = (-51.1 \pm 5.9)\ J\,mol^{-1}K^{-1}$ from an Eyring plot (see Supporting Information, Figure S19 – S24), and the experimental barrier is in excellent agreement with that computed with DFT, see below (computed $\Delta G^{\neq} = 52\ kJ\,mol^{-1}$). In order to support the assignment of the slower decay process of the ferryl oxidant as the demethylation reaction, the self-decay kinetics of $[(L^{1a})Fe^{IV}=O(Cl)]^+$, i.e. the precursor that does not have a methyl group at N3, was also measured. Note, that $[(L^{1a})Fe^{IV}=O(Cl)]^+$ obviously has slightly different electronic properties (i.e. a different ligand field and hence a different triplet-quintet energy gap), and this is confirmed by its electronic spectrum shown in Figure 5c (absorption maximum at 815 nm vs. 850 nm). Therefore, the decay of the ferryl complex was significantly slower and measured at a higher temperature. The comparison with the time trace of $[(L^{1})Fe^{IV}=O(Cl)]^+$ shows impressively the effect on the stability of the iron(IV)-oxido complex when preventing the demethylation decay path (see Figure 5d).

In order to qualitatively probe the importance of ligand field effects, we have also prepared the bromido-ferryl complex of L^1 and compared its decay rate in preliminary experiments with that of the analogous chlorido-ferryl complex studied here in detail (see Figure 6a for the electronic spectra and Figure 6b for a comparison of the two time-traces). The low energy dd transition of $[(L^{1})Fe^{IV}=O(Br)]^+$, associated with the transition to $d_{x2\text{-}y2}$, is shifted by 50 nm to lower energy with respect to that of $[(L^{1})Fe^{IV}=O(Cl)]^+$ (900 nm vs. 850 nm), indicating a lower in-plane ligand field and this leads to a concomitant increase of the decay rate by about one order of magnitude (see Figure 6b).[50] In a previous publication, we already showed a similar effect on reactivity when comparing the complexes with MeCN and Cl^- as co-ligand,[30] where a shift of the absorption maxima by about 80 nm to lower wavelengths was observed (see Figure 6a), as well as a 2000-fold decrease of the decay rate compared to the Cl^- complex. Similar though less pronounced effects were observed with the $Fe^{IV}=O$ complexes of a pyridyl-substituted triazacyclononane ligand (Pytacn), also leading to a *cis*-disposition of the monodentate co-ligand (MeCN, Cl^-, Br^-) with respect to the oxido group,[51] where the MeCN complex has a 53 nm higher energy $d_{x2\text{-}y2}$ transition than the Cl^- complex, which is 20 nm higher in energy than for the Br^- species (750 nm vs. 803 nm vs. 823 nm), and the chloride and bromide complexes are a factor 2 to 3 more reactive in C–H abstraction from 9,10-dihydroanthracene.

While the MeCN complex was known to have $S=1$ electronic configuration, due to the extreme reactivity, the chlorido-ferryl complex could only recently be trapped by cryo-stopped-flow experiments. The DFT-based predictions erroneously supported circumstantial earlier evidence for an $S=2$ ground state, and this could now be clarified.[30] The interesting observation that the chlorido and more so the bromido complexes are the most reactive ferryl complexes known so far, more reactive than $S=2$ model systems and at least as reactive as some nonheme iron enzyme systems, raises the question of the origin of this reactivity.[37] While a thorough answer to this question requires further experimental and theoretical studies, it is interesting that the triplet-quintet gaps, qualitatively related the dd absorption maxima assigned to the $d_{xz/yz}, d_{xy} \rightarrow d_{x2-y2}$ transitions at 768 nm, 850 nm and 900 nm for the MeCN, Cl^- and Br^- based ferryl complexes, respectively, correlate qualitatively with the computed triplet-quintet energy differences of 75.7 kJ/mol and 5.7 kJ/mol for the MeCN and the Cl^- based oxidants, respectively, and a small energy difference to the quintet spin surface leads – as expected – to high activity.

Double-mixing experiments with cyclohexane were performed to investigate the reactivity of $[(L^{1})Fe^{IV}=O(Cl)]^+$ with respect to C–H abstraction (EtCN, 183 K). The iron(II) precursor was oxidized with ^{s}PhIO, and cyclohexane (15 equiv.) was injected after reaching the maximum absorption (after 3 s), which leads to a fast decay of the dd transition at 850 nm with the observed rate constant $k_4 = 0.20 \pm 0.02\ s^{-1}$.[52] A first cautious estimate of the second-order rate can be obtained by varying the lag time between mixing of the Fe^{II} precursor and the ^{s}PhIO oxidant, and the addition of the cyclohexane substrate, i.e. the concentration of $[(L^{1})Fe^{IV}=O(Cl)]^+$ depends on the formation and the two self-decay rates (see Supporting Information, Figure S25–S27, Table S11). Admittedly, the resulting rate cannot be regarded as very precise but with a value of $k_4 = (7.55 \pm 0.27) \cdot 10^2\ M^{-1}s^{-1}$ this suggests a significantly higher reactivity in C–H activation than previously known iron(IV)-oxido complexes, especially since our measurements relate to lower temperatures than those observed before.[32,53,54]

An overview of the preliminary kinetic data is given in Table 1 (see Scheme 2 for the numbering of the reaction paths). Admittedly, this analysis is limited by the fact that not all reactions are studied under identical conditions, and a more thorough and complete analysis for k_4 is in progress. However, these data allow the conclusions that (i) the kinetic analysis confirms the results of the MS experiments and shows a self-decay of the ferryl complex via a fast second-order reaction that can be attributed to the formation of an oxido-bridged diiron complex and a parallel slower first-order reaction, attributed to an intramolecular demethylation process; (ii) ligand field effects for example due to a variation of the co-ligand or coordination of a secondary instead of a tertiary amine have a huge impact

Table 1. Overview of the determined rate constants of the reaction of $[(L^{1})Fe^{II}Cl_2]$ with ^{s}PhIO at 183 K in EtCN and with further addition of cyclohexane as substrate (the values in square brackets and italics (pseudo-first-order rate of k_1 and second order rate of k_4) are derived with approximations and therefore are less accurate and have to be considered with caution, see text; the value for k_2 is only a rough estimate, see text and Supporting Information, Figure S17).

reaction rates
$k_1 = [1.2\ s^{-1}]\ (1.48 \pm 0.06) \cdot 10^3\ M^{-1}s^{-1}$
$k_2 \leq k_{dinucl.} = (0.13 \pm 0.01)\ s^{-1}$
$k_3 = (5.82 \pm 0.59) \cdot 10^{-3}\ s^{-1}$
$k_4 = 0.20 \pm 0.02\ s^{-1}\ [(7.55 \pm 0.27) \cdot 10^2\ M^{-1}s^{-1}]$

on the reactivity; (iii) $[(L^1)Fe^{IV}{=}O(Cl)]^+$ shows the highest reactivity ever observed in C–H abstraction of cyclohexane – importantly, this HAA process selectively forms the chlorinated product as shown below.

DFT analysis

Density functional theory (DFT) calculations were used to compute plausible pathways for the demethylation of the coordinated bispidine L^1 at N7 (only the *trans*-N3 isomer was considered, the corresponding *trans*-N7 isomer is known to be less stable,[48] and the experimental data (see sections on mass spectrometry and bulk reactions) show that the relevant isomer has *trans*-N3 configuration). Similar intramolecular HAA reactions were described for other ligand-based processes induced by high-valent metal-oxido species.[42,43,46,48] The intramolecular ligand decay starts with the oxido-group of $[(L^1)Fe^{IV}{=}O(X)]^{n+}$ ($X = Cl^-$, MeCN), *R*, abstracting a hydrogen atom from the methyl group at N7 via transition state *ts1*, producing *int1*, an Fe^{III}-hydroxido intermediate with a ligand-based radical, $[(L\text{-}H^{\bullet})Fe^{III}\text{-}OH(X)]^{n+}$ (see Scheme 3). An intramolecular radical rebound step then leads via *ts2* to the Fe^{II} intermediate *int2* with a 4-membered amino alcohol chelate involving N7 (note that a derivative of this intermediate was observed by mass spectrometry). From *int2*, there are two possible routes: in pathway *a*, there is heterolytic cleavage of the C–N7 bond in the 4-membered ring, leading over *ts3a* to the six-coordinate Fe^{II} intermediate *int3a* with a coordinated amide anion. Product *P*, the iron precatalyst $[(L^1)Fe^{II}(X)]^{n+}$ ($X = Cl^-$, MeCN), and CH_2O are then produced either in a concerted reaction or via two proton transfer steps via *int3a'*. In the alternative pathway *b*, the alcohol coordinated to Fe^{II} is released (*int3b* via *ts3b*), and a concerted proton transfer leads to *P* and CH_2O.

The computed free energy profile of the demethylation process of $[(L^1)Fe^{IV}{=}O(Cl)]^+$, involving the three spin surfaces starting with the singlet, triplet and quintet ferryl species and including both pathways *a* and *b* is shown in Figure 7 – the corresponding plot for $[(L^1)Fe^{IV}{=}O(MeCN)]^{2+}$ is given as Supporting Information (Figure S31; plots of the optimized structures of all relevant intermediates and transition states, together with selected structural data, as well as computed spin densities are given in Figures S33–S39). Note that DFT generally has problems in predicting the correct spin state energies,[55–60] and a recent DLPNO-CCSD(T) study, also involving $[(L^1)Fe^{IV}{=}O(X)]^{n+}$ ($X = Cl^-$, MeCN) shows in agreement with experimental data that the DFT computed spin ground states of the ferryl complexes are, not unexpectedly, wrong.[30] As usual, we assume, that the computed activation barriers for the various pathways are nevertheless of acceptable accuracy.

The estimated barrier height for the rate determining C–H abstraction step at the methyl group of N7 is rather low for the

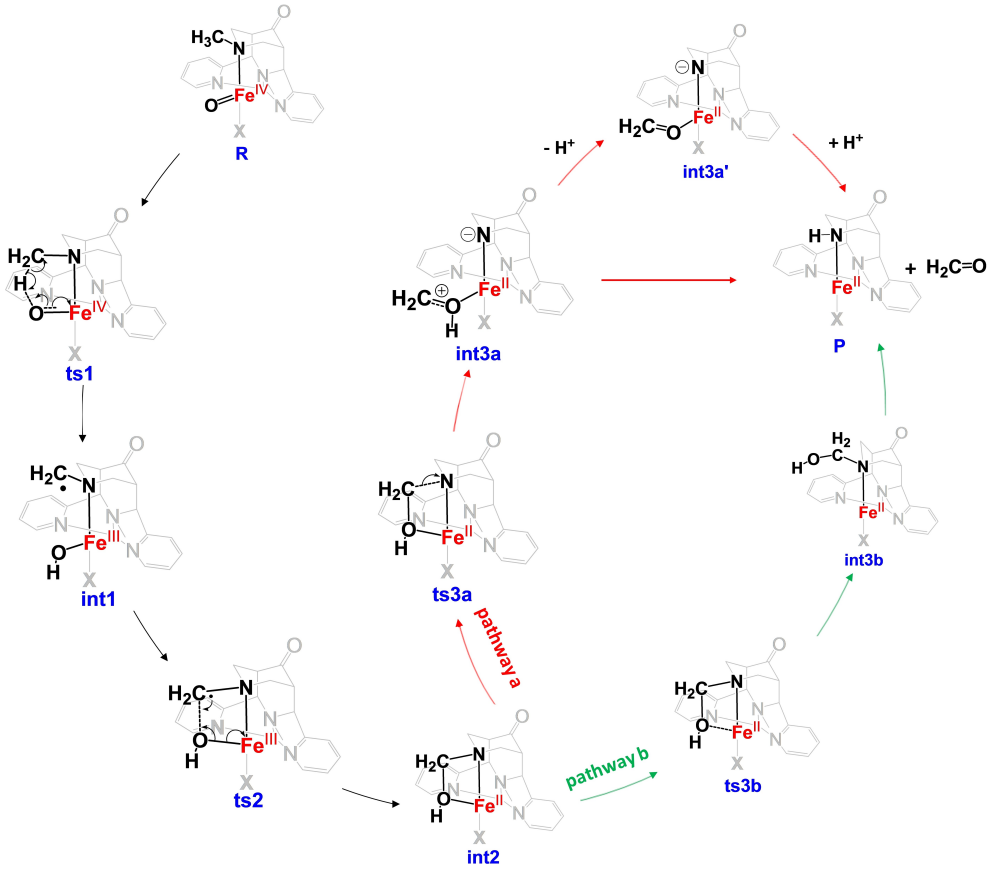

Scheme 3. Proposed demethylation/formaldehyde formation mechanism of $[(L^1)Fe^{IV}{=}O(X)]^{n+}$ ($X = Cl^-$, MeCN).

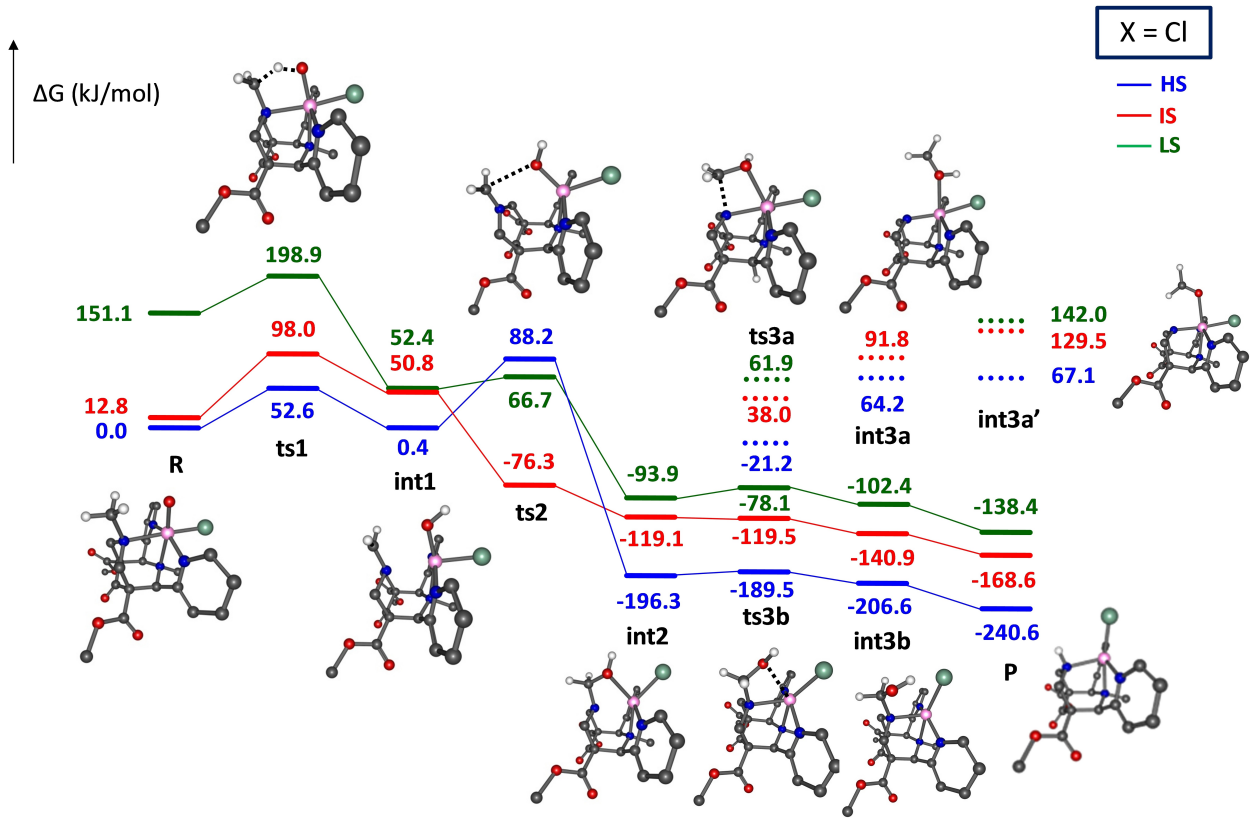

Figure 7. Free energy profile for the demethylation of the bispidine based $[(L^1)Fe^{IV}=O(Cl)]^+$ complex.

chlorido complex (approx. 50 kJ/mol) and significantly higher for the MeCN-based reactant (approx. 80 kJ/mol), indicating that the chlorido complex is exceedingly reactive and that the MeCN complex still is an efficient but much slower oxidant. The computed activation barrier for the rebound process is predicted to proceed over an $S=1$ transition state to the rather stable cyclic rebound intermediate *int2*. Not unexpectedly, the strain in the four-membered ring is released at the relatively weak Fe^{II}-alcohol bond, i.e. pathway *b* is energetically favored. A series of fast steps then leads to the iron(II) catalyst resting state $[(L^1)Fe^{II}(X)]^{n+}$ ($X=Cl^-$, MeCN) and the CH_2O product. In earlier studies on cyclohexane halogenation catalyzed by $[(L^1)Fe^{IV}=O(Cl)]^+$, the free energy activation barrier for C–H abstraction from cyclohexane (rate-determining step) was computed with a slightly different DFT method to be around 50 kJ/mol, comparable to the values obtained here.[21] More accurate studies in progress indicate that the barrier of the intermolecular HAA is lower than the intramolecular process described here, and this is in agreement with the kinetic data above. For cyclohexane hydroxylation with $[(L^1)Fe^{IV}=O(OH)]^+$, the computed activation free energy was nearly 15 kJ/mol higher,[24] demonstrating the efficiency of the chlorido complex and supporting the importance of the ligand field strength of the monodentate coligand (see kinetic data and dd spectra of the corresponding ferryl complexes above).

Bulk reactions

Bulk reactions with $[(L^n)Fe^{IV}=O(Cl)]^+$ ($n=1,2,3$) in presence of cyclohexane were performed in support of the proposed mechanism. As in the ESI-MS experiments, the two benzylated ligand derivatives were used to assess whether the self-decay process (demethylation/debenzylation) is an intra- or intermolecular process. Therefore, benzaldehyde formation and, in addition, the halogenation of cyclohexane were studied quantitatively by gas chromatography (GC, see Table 1; see Supporting Information for reaction conditions).[38] The data in Table 1 confirm the results from the MS experiments and the mechanistic proposal derived from the DFT study: with the $[(L^2)Fe^{II}Cl_2]$ precursor, there is formation of benzaldehyde (max. approx. 50% with respect to the iron precatalyst), while with $[(L^3)Fe^{II}Cl_2]$ no benzaldehyde is detected. We take this as evidence for an intra- rather than an intermolecular process for the ligand degradation. Importantly, this also confirms the DFT-based suggestion that the active ferryl oxidant has the oxido-group trans to N3.[12,19,48]

As expected from earlier work[21] and from the kinetic analysis above, the data in Table 2 also show that chlorocyclohexane is produced in the presence of excess cyclohexane and, as noted before,[21] the halogenation is selective, i.e. neither cyclohexanol nor cyclohexanone were observed, and similar amounts of chlorocyclohexane are formed with all L^n complexes ($n=1$–3)). As expected from earlier work,[20,24] with MeCN

Table 2. Yield of the products from the reaction of $[(L^n)Fe^{II}Cl_2]$ (7 mM, n = 1-3) with ^{s}PhIO (10 eq) and with cyclohexane (100 eq) as substrate in MeCN after 1 or 24 h stirring under Ar atmosphere at ambient temperature (the percentages are with respect to the amount of iron precatalyst used).

complex	t [h]	cyCl [%]	PhCHO [%]
$[(L^1)Fe^{II}Cl_2]$	1	22.4 ± 0.4	–
$[(L^2)Fe^{II}Cl_2]$	1	27.8 ± 3.9	48.6 ± 6.0
$[(L^3)Fe^{II}Cl_2]$	1	28.6 ± 0.1	0
$[(L^1)Fe^{II}Cl_2]$	24	47.0 ± 4.3	–

instead of Cl^- as co-ligand cyclohexanol instead of chlorocyclohexane is the main substrate oxidation product (a thorough study of the halogenation reaction will be published separately). Measurements at longer reaction times than 1 h show that the formation of benzaldehyde does not increase further. From the time-dependent formation of chlorocyclohexane ($[(L^1)Fe^{II}Cl_2]$: ^{s}PhIO: cyclohexane = 1:10:100, see Figure 8) however, it is concluded that chlorocyclohexane formation under these conditions is significantly slower, i.e. the final yield of approx. 45% with respect to the iron(II) precursor is only reached after 24 h.

A disturbing but most interesting observation is that the lifetime of $[(L^1)Fe^{IV}=O(Cl)]^+$ is very short, *viz.* seconds at −90 °C (see section on kinetics), while the reactions discussed here (bulk dealkylation of the ligand and selective halogenation of cyclohexane) are studied at ambient temperature over hours. There are two corollaries, and these are now discussed in detail: (i) C–H abstraction from cyclohexane by $[(L^1)Fe^{IV}=O(Cl)]^+$ is to a large extent unproductive and (ii) the slow formation of chlorocyclohexane (see Figure 8) must emerge from another pathway.

(i) The putative direct oxidation of cyclohexane by $[(L^1)Fe^{IV}=O(Cl)]^+$ via a selective rebound process produces chlorocyclohexane and $[(L^1)Fe^{II}(X)(Y)]^{n+}$ (X, Y = Cl^-, OH^- or MeCN). The rate-determining hydrogen abstraction forms a cyclohexyl radical and $[(L^1)Fe^{III}(Cl)(OH)]^+$, followed by the rebound of the cyclohexyl radical to the Fe^{III}-Cl intermediate. From the cryo-stopped-flow kinetic analysis it follows that the three competing decay processes of $[(L^1)Fe^{IV}=O(Cl)]^+$ under similar conditions (EtCN, 183 K, $[(L^1)Fe^{II}(Cl)_2]$: ^{s}PhIO : cyclohexane = 1:2:15) have pseudo-first-order rate constants of approx. $k_2 = 1\cdot10^{-1}\ s^{-1}$ (formation of the oxido-bridged diiron(III) product), $k_3 = 6\cdot10^{-3}\ s^{-1}$ (demethylation), and $k_4 = 2\cdot10^{-1}\ s^{-1}$ (halogenation, see Table 1). In a stoichiometric reaction one therefore would expect around 60% halogenation, 30% formation of the $[Cl(L^1)Fe^{III}\text{-}O\text{-}Fe^{III}(L^1)Cl]^{2+}$ "resting state" and only traces of dealkylation products (note however that these are only rough estimates; for example the "dimerization" rate might be overestimated, see section on kinetics). The fact that only minor amounts of halogenation products are observed initially in the ambient temperature reaction (see Figure 8) indicates that most of the formed cyclohexyl radicals (we assume at least 90%) decay unproductively, i.e. via "cage escape", where the cyclohexyl radicals abstract a hydrogen atom from the solvent or excess substrate.[61–63] An often used test for "cage escape" is to investigate changes of the product distribution in HAA and OAT reactions under strict exclusion or in presence of dioxygen;[19,20,24,62,64] O_2 can trap organic radicals and, with HAA from alkane substrates, the resulting alkylperoxides form the alcohol and ketone products with a Russel-type mechanism in a 1:1 ratio.[65] Indeed, under ambient atmosphere a mixture of chlorocyclohexane, cyclohexanol and cyclohexanone is observed (see Supporting Information, Table S6). Since O_2 may also react with some of the iron intermediates, which might lead to changes in the product distribution, we have also performed halogenation reactions in presence of TEMPO (2,2,6,6-tetramethylpiperidinyloxyl), which is also known to trap organic radicals. The reaction products with hydrogen atoms (deuterium when perdeuterated cyclohexane was used), methyl radicals and cyclohexyl radicals were identified in MS experiments and, in presence of 10 equivalents of TEMPO, the halogenation was completely quenched under the usual reaction conditions (see Supporting Information for details, Tables S8 and S9). We take this as evidence for a "cage escape" pathway although we suggest that "cage escape" may give the wrong impression because the concentration dependence of the second order quenching process of the substrate radical indicates that the quencher (TEMPO or O_2 or cyclohexane) rather enters the cage than the cyclohexyl radical escapes it. This also emerges from earlier mechanistic studies on the bispidine-iron-induced epoxidation of cyclooctene.[19,25,64] However, the common observation is that the efficiency of both these non-rebound pathways increase with increasing lifetime of the $[(L^1)Fe^{III}(OH)(Cl)]^+$cyclohexyl radical intermediate, i.e. with an increase of the rebound energy barrier, and the barrier in the ferryl systems discussed here is substantial. Note however, that cage escape has only been substantiated in the bulk reaction – for technical reasons, product analysis was not possible in the cryo-stopped-flow experiments. That is, our interpretation assumes the same $[(L^1)Fe^{IV}=$

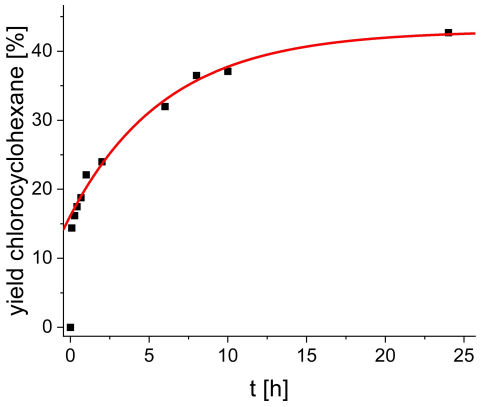

Figure 8. Time-dependent formation of chlorocyclohexane in the reaction of $[(L^1)Fe^{II}Cl_2]$ (7 mM) with ^{s}PhIO (10 eq) and with cyclohexane (100 eq) as substrate in MeCN, stirred under Ar atmosphere at ambient temperature. The percentages are based on the amount of iron(II) precursor. The red line is an arbitrary exponential function to guide the eye and indicate that chlorocyclohexane formation is due to processes with very different rates.

$O(Cl)]^+$ oxidant in the low temperature kinetics and the ambient temperature batch reactions.

(ii) The exceedingly fast decay of $[(L^1)Fe^{IV}=O(Cl)]^+$ in presence of cyclohexane, due to a large ratio of "cage escape", i.e. unproductive cyclohexyl radicals, mainly produces $[Cl(L^1)Fe^{III}\text{-}O\text{-}Fe^{III}(L^1)Cl]^{2+}$ and some $[(L^{1a})Fe^{II}(MeCN)(Cl)]^+$. The latter (the N7-demethylated iron(II) precursor) has a similar reactivity to that of the L^1 based complex, i.e. it primarily produces the corresponding oxido-bridged diiron(III) complex (see also section on kinetics above). This is a consequence of the conditions for the bulk reaction: due to requirements for the product analyses (detection limit of GC), the concentration of the iron precursor must be of the order of 7 mM, and the maximum solubility of ^{s}PhIO is 4 mM. Therefore, at the beginning of the process, the concentration of oxidant is lower than that of the iron precursor. According to the MS experiments and kinetic analyses this strongly promotes the formation of the oxido-bridged diiron(III) complex. Another important observation is that addition of excess Cl^- leads to reduced yields of chlorocyclohexane, and this is shown to be due to oxidation of Cl^- to ClO^- by the ferryl oxidant.[49] This is supported by the fact that the dealkylation process selectively leads to oxygenated products (see section on mass spectrometry). Therefore, the chlorocyclohexane product must arise from an Fe–Cl based species, i.e. a rebound pathway. It follows that after a short initial phase, most of the products observed in the bulk reactions (benzaldehyde and chlorocyclohexane) emerge from $[Cl(L^1)Fe^{III}\text{-}O\text{-}Fe^{III}(L^1)Cl]^{2+}$ (and its L^{1a} based derivative). The conclusion is that, in the catalytic halogenation reaction described in this section, most of the chlorocyclohexane is produced by $[Cl(L^1)Fe^{III}\text{-}O\text{-}Fe^{III}(L^1)Cl]^{2+}$ as the precatalyst, and we assume that, in presence of ^{s}PhIO this produces in a very slow reaction the ferryl complex as the active catalyst (see Scheme 4).

Conclusion

The data discussed here show that $[(L^1)Fe^{IV}=O(Cl)]^+$ has the oxido-group *trans* to N3 (see Scheme 1) and an $S=1$ electronic ground state,[30] and that, regardless of the "wrong" spin ground state of the ferryl complex, $S=1$ $[(L^1)Fe^{IV}=O(Cl)]^+$ has the highest reactivity for HAA reactions catalyzed by known ferryl complexes. Also, $[(L^1)Fe^{IV}=O(Cl)]^+$ is believed to have (one of) the highest $Fe^{IV/III}=O$ redox potentials although one needs to be cautious with reported $Fe^{IV/III}$ potentials.[66] An interesting question is, how much the observed reactivity relates to the $Fe^{IV/III}$ potential, how much to the electrophilicity of the oxido-group and how much it depends on the quintet-triplet gap of the ferryl complex. We believe to have shown with the data presented here that some of these interesting questions may be discussed thoroughly with the bispidine-based complexes studied here.

An initially annoying but important observation is that the exceedingly high reactivity of $[(L^1)Fe^{IV}=O(Cl)]^+$ is unproductive, i.e. leading to the unwanted side products $[Cl(L^1)Fe^{III}\text{-}O\text{-}Fe^{III}(L^1)Cl]^{2+}$ and $[(L^{1a})Fe^{II}(MeCN)(Cl)]^+$ rather than to chlorocyclohexane and $[(L^1)Fe^{II}(MeCN)(Cl)]^+$. Demethylation can be prevented by using $[(L^{1a})Fe^{II}(Cl)_2]$ as precatalyst, and preliminary experiments indicate that the L^{1a} based oxidant has a similar reactivity (note that for a number of reasons it might be of advantage to use ligand derivatives that are N3 as well as N7 demethylated and with reduced C9 ketone and hydrolyzed C1, C5 ester groups, and these ligands are all available and assumed to lead to ferryl complexes with similar reactivity). There are possibilities to prevent formation of the oxido-bridged diiron(III) complexes (e.g. by reactions at very high dilution or with more elaborate systems involving fixation of the iron(II) precursors at a distance that prevents interaction of the iron sites). Studies in these directions may show whether an efficient and stable catalyst may then be produced.

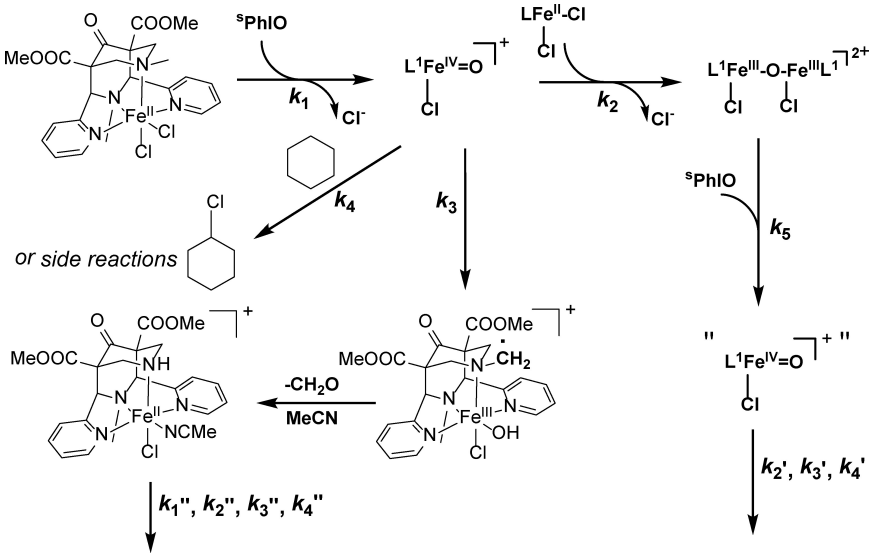

Scheme 4. Formation of $[(L^1)Fe^{IV}=O(Cl)]^+$ (k_1), its decay to the oxido-bridged diiron(III) complex (k_2), decay by Fe^{III} C–H activation leading to demethylation (k_3), substrate (cyclohexane) oxidation (k_4), and assumed reactivity involving the "self-decay" products.

Experimental Section

Materials and methods

All chemicals and reagents were purchased from commercial sources (ABCR; ACROS, Sigma-Aldrich; TCI). Dry solvents were stored over molecular sieves and, with the exception of propionitrile, were used without further purification. Purchased propionitrile contains impurities such as isocyanate or cyanate ions, which can interfere with the reactions by coordinating to the complexes used. For purification, propionitrile was first extracted with aqueous HCl solution (20%, 2x) and then with a saturated $NaHCO_3$ solution (3x). The solvent was then pre-dried by addition of Na_2SO_4. After filtration of the solid, it was carefully dried over CaH_2. After filtration and addition of fresh CaH_2, the solvent was refluxed for 1 day, followed by distillation and storage over molecular sieve (4 Å). Preparation and handling of air-sensitive materials were carried out using either Schlenk techniques or in a glovebox under Ar atmosphere.

MS experiments were carried out on a ApexQe hybrid 9.4 T FT-ICR from Bruker. For HR-ESI and tandem MS measurements with various oxidant concentrations the samples were prepared in the glove box. The measured solutions had iron complex-concentrations of 10^{-5} M in abs. MeCN. Corresponding amounts of oxidant were added. The reactions were carried out in a total reaction volume of 2 mL. The reactions were stirred 1 h at rt. Then, 1 mL of the reaction solution was taken, filtered through a syringe filter and filled into a vial with septum. Then the measurements were carried out by the Mass Spectromety Facility, Department of Chemistry, University of Heidelberg, Heidelberg, Germany.

Elemental analyses were performed on a CHN–O Vario EL by the "Mikroanalytisches Labor", Department of Chemistry, Heidelberg University, Heidelberg, Germany.

UV – vis – NIR spectra were recorded on an Agilent 8453 spectrophotometer equipped with an *USP-203-A* cryostat from Unisoku. Spectra were processed with Origin 2019.

X-ray crystallography: see the Supporting Information for the details of the crystal structure determinations. Plots of the crystal structure shown in this publication were performed using the programs *ORTEP* and *POV-Ray*.

Kinetik measurements: cryo-stopped-flow measurements were performed with a SFM-4000/S stopped flow mixer from Bio-Logic Science Instruments. The UV-vis spectra were recorded by using a Tidas MCS UV/NIR from J&M Analytik AG and the temperature was controlled by a Thermo Scientific Phoenix II cryostat. Rate constants were obtained either by fitting the data with the software OriginPro 2018G or via global analysis with the software ReactLab KINETICS by Jplus Consulting.

Bulk reaction to determine benzaldehyde and chlorocyclohexane formation were carried out in the glovebox with iron complex concentrations of 7 mM and a total reaction volume of 2 mL (MeCN). To the iron complex, cyclohexane (100 eq) and ^{s}PhIO (10 eq) were added and after stirring at room temperature for 1 h, to the reaction mixture the internal standard nitrobenzene for the GC measurement was added. Then, the reaction solution was filtered over a pipette column (silica) to remove the iron catalyst. The column was rinsed with 3 mL MeCN. The GC measurements were carried out with a Varian 3900.

Experiments with TEMPO were carried out with iron complex (7 mM), cyclohexane (700 mM), PhIO (70 mM) and TEMPO (70 mM), which were added subsequentially to 2 ml abs. MeCN under Ar atmosphere and stirred for 24 h at rt. To separate the iron complex, the reaction mixture was filtered through a pipette column (silica) and rinsed with 3 ml MeCN. Product analysis was carried out with an Ultra Trace GC from Thermo Fischer (TG-1701MS column, 30 m, 0.25 mm, 0.25 μm) with a Single Quadropole MS detector. Helium was used as a carrier gas and electron ionization was used as an ionization method.

Syntheses

The bispidine-iron(II) complex and soluble iodosylbenzene (^{s}PhIO) were synthesized according to literature procedures.[21,67–73] The chloride/bromido complexes were prepared as follows: Iron(II) chloride or iron(II) bromide (6.36 mmol) was added to a solution of the bispidine ligand (6.36 mmol) in dry acetonitrile (60 mL) under nitrogen atmosphere. After one hour stirring at room temperature, the precipitated complex was filtered and dried under vacuum.

$[(L^2)Fe^{II}(Cl)_2]$ (640.09 g/mol, $C_{29}H_{30}Cl_2FeN_4O_5$): HR-ESI MS (pos, MeOH): $[(L^2)Fe^{II}(Cl)]^+$ calcd. 605.1249, obsd. 605.1264 (100%). Elem. Anal. (report no. 43066). Calcd for $[[(L^2)Fe^{II}(Cl)_2]$ MeCN]: C 54.57, H 4.87, N 10.26%. Obsd: C 54.34 H 4.52, N 10.64%. UV – vis – NIR (MeCN, rt): λ [nm] (ε [M^{-1} cm^{-1}]) 427 (2149).

$[(L^3)Fe^{II}(Cl)_2]$ (640.09 g/mol, $C_{29}H_{30}Cl_2FeN_4O_5$): HR-ESI MS (pos, MeOH): $[(L^3)Fe^{II}(Cl)]^+$ calcd. 605.1249, obsd. 605.1258 (100%). Elem. Anal. (report no. 43303). Calcd for $[[(L^2)Fe^{II}(Cl)_2]$ 0.5 MeCN]: C 54.44, H 4.80, N 9.52%. Obsd: C 54.36 H 4.95, N 9.54%. UV-vis-NIR (MeCN, rt): λ [nm] (ε [M^{-1} cm^{-1}]) 413 (1974).

$[(L^{1a})Fe^{II}(Cl)_2]$ (551,20 g/mol, $C_{22}H_{24}Cl_2FeN_4O_5$): HR-ESI MS (pos, MeCN): $[(L^{1a})Fe^{II}(Cl)]^+$ calcd. 515.0779, obsd. 515.0775 (100%). Elem. Anal. (report no. 45185). Calcd for $[(L^{1a})Fe^{II}(Cl)_2]$: C 47.94, H 4.39, N 10.16%. Obsd: C 47.63, H 4.52, N 10.21%.

$[(L^1)Fe^{II}(Br)_2]$ (651.96 g/mol, $C_{23}H_{26}Br_2FeN_4O_5$): HR-ESI MS (pos, MeCN): $[(L^1)Fe^{II}(Br)]^+$ calcd. 573.0431, obsd. 573.0432 (100%). Elem. Anal. (report no. 45967). Calcd for $[[(L^1)Fe^{II}(Br)_2]$ 0.5 H_2O 0.5 MeCN]: C 42.16, H 4.20, N 9.22%. Obsd: C 42.20, H 4.34, N 9.16%.

Crystals of the iron complexes were obtained from concentrated solutions in MeCN at ambient temperature.

$[(L^{1a})Fe^{II}(Br)_2]$. $FeBr_2$ (762 mg, 3.5 mmol, 1.0 eq.) was added to a suspension of L^{1a} (1.511 g, 3.6 mmol, 1.0 eq.) in abs. MeCN (10 ml) under N_2 atmosphere and stirred for 16 h at RT. The suspension was filtered, the residue was washed with cold abs. MeCN (3 ml, 2x) and then dried in high vacuum to obtain the product as brown solid. The filtrate and washing solutions were combined, layered with abs. Et_2O (30 ml) and stored at RT. Crystal structures for $[Fe(L^{1a})(Br)_2]$ and $\{[Fe^{III}L^{1a}\text{-}(OH)_2)]_2(O)(Br)_2\}(Br)_2]$ were obtained. The cause of the dimerization and hydration is probably $FeBr_2$ contaminated with water, which was used as educt. $[(L^{1a})Fe^{II}(Br)_2]$ (640.11 g/mol, $C_{22}H_{24}Br_2FeN_4O_5$): HR-ESI MS (pos, MeCN): $[(L^{1a})Fe^{II}(Br)]^+$ calcd. 559.0274, obsd. 559.0282 (100%). Elem. Anal. (report no. 45184). Calcd for $[[(L^{1a})Fe^{II}(Br)_2]$ H_2O]: C 40.15, H 3.98, N 8.51%. Obsd: C 40.06, H 4.10, N 8.41%.

$[(L^2)Fe(MeCN)_2](BF_4)_2$.$[(L^2)Fe^{II}(Cl)_2]$ (1.56 mmol, 1.00eq) was dissolved in 15 ml abs. MeCN under ar. $Ag(BF_4)$ (4.13 mmol, 2.6eq) was added and the solution was stirred overnight. After filtration and crystalisation, the product was obtained as greenish solid (0.79 mmol, 50.6%). $[[(L^2)Fe^{II}(BF_4)_2]2$ MeCN] (826.22 g/mol, $C_{33}H_{36}B_2F_8Fe_6O_5$): HR-ESI MS (pos, MeOH): $[(L^2)Fe^{II}(F)]^+$ calcd. 589.1544, obsd. 589.1551 (100%). Elem. Anal. (report no. 43923). Calcd for $[[(L^2)Fe^{II}(BF_4)_2]2$ MeCN, 0.6 BF_2OH]: C 45.79, H 4.26,N 9.71%. Obsd: C 45.46, H 4.30, N 10.03%.

Computational methods

The molecular structures of all the intermediates and transition states involved in the self-decay mechanism of bispidine based $Fe^{IV}=O$ complexes were fully optimized in all possible spin states using spin-

unrestricted B3LYP functional.[74–76] Based on earlier studies, with the exchange–correlation hybrid B3LYP functional reliable and accurate electronic structures and energetics, particularly of bispidine-based transition metal complexes are expected.[22,23,55,77–79] The double-ζ quality Los Alamos national laboratory (LANL2DZ)[80,81] effective core potential was employed to describe the Fe center and the 6–31G (d,p)[82] basis set was used for H, C, N, O and Cl. Vibrational frequencies were computed to extract thermodynamic details and to verify the nature of the stationary points. The gas-phase energies were further improved by performing single-point calculations on the optimized geometries with triple-ζ valence polarization (TZVP)[83] basis sets for all atoms including the effect of MeCN solvent. The self-consistent reaction field-polarizable continuum model (SCRF-PCM)[84–87] was employed to incorporate implicit solvent effects. The solvation energies were added with free energy corrections extracted from the frequency calculation on the corresponding gas-phase optimized geometries. Therefore, all free energies quoted in present study are those obtained from PCM (NCMe) B3LYP/TZVP//B3LYP/LANL2DZ(6-31G(d,p) level of theory at 1 atm and 298.15 K. The quadratic convergence keyword was used to facilitate a smooth SCF procedure. NBO analyses[88,89] were carried out with wave functions generated at the B3LYP/LANL2DZ(6-31G(d,p) level of theory. The Gaussian09 code was used for performing all computations.[90]

Supporting Information

The Supporting Information includes further experimental and computational details, specifically with respect to the MS, GC, GC-MS and kinetic experiments. It also includes details of the crystal structure analyses. Deposition Numbers 2055798, 2055799, 2055800, and 2055801 contain the supplementary crystallographic data for this paper. These data are provided free of charge by the joint Cambridge Crystallographic Data Centre and Fachinformationszentrum Karlsruhe Access Structures service.

Acknowledgements

Financial support by Heidelberg University, the European Cooperation in Science and Technology (COST) and the German Science Foundation (DFG) is gratefully acknowledged. This study was conducted within the Max Planck School Matter to Life, supported by the German Federal Ministry of Education and Research (BMBF) in collaboration with the Max Planck Society. We also acknowledge support by the state of Baden-Württemberg for an LGF bursary to K.B. and for computer resources on bwHPC, supported by the German Science Foundation (DFG) through grant no INST 40/467-1 FUGG (JUSTUS cluster). Open access funding enabled and organized by Projekt DEAL.

Conflict of Interest

The authors declare no conflict of interest.

Keywords: C–H activation · mass spectrometry · nonheme iron · reaction mechanism · stopped-flow kinetics

[1] C. A. Grapperhaus, B. Mienert, E. Bill, T. Weyhermüller, K. Wieghardt, *Inorg. Chem.* **2000**, *39*, 5306–5317.
[2] J. C. Price, E. W. Barr, B. Tirupati, J. M. Bollinger Jr., C. Krebs, *Biochemistry* **2003**, *42*, 7497.
[3] J.-U. Rohde, J.-H. In, M. H. Lim, W. W. Brennessel, M. R. Bukowski, A. Stubna, E. Münck, W. Nam, L. Que Jr., *Science* **2003**, *299*, 1037–1039.
[4] C. Krebs, D. Galonici Fujimori, C. T. Walsh, J. M. Bollinger Jr., *Acc. Chem. Res.* **2007**, *40*, 484–492.
[5] W. Nam, Y.-M. Lee, S. Fukuzumi, *Acc. Chem. Res.* **2014**, *47*, 1146–1154.
[6] E. I. Solomon, T. C. Brunold, M. I. Davis, J. N. Kensley, S.-K. Lee, N. Lehnert, F. Neese, A. J. Skulan, Y.-S. Yang, J. Zhou, *Chem. Rev.* **2000**, *100*, 235.
[7] M. M. Abu-Omar, A. Loaiza, N. Hontzeas, *Chem. Rev.* **2005**, *105*, 2227–2252.
[8] P. Comba, M. Kerscher, M. Krause, H. F. Schöler, *Env. Chem.* **2015**, *12*, 381–395.
[9] J. M. Mayer, *Acc. Chem. Res.* **2011**, *44*, 36–46.
[10] D. Wang, K. Ray, M. J. Collins, E. R. Farquhar, J. R. Frisch, L. Gomez, T. A. Jackson, M. Kerscher, A. Waleska, P. Comba, M. Costas, E. Münck, L. Que Jr., *Chem. Sci.* **2013**, *4*, 282–291.
[11] P. Comba, H. Wadepohl, A. Waleska, *Aust. J. Chem.* **2014**, *67*, 398–404.
[12] P. Comba, S. Fukuzumi, C. Koke, A. M. Löhr, J. Straub, *Angew. Chem. Int. Ed.* **2016**, *55*, 11129–11133.
[13] S. Shaik, D. Danovich, A. Fiedler, D. Schröder, H. Schwarz, *Helv. Chim. Acta* **1995**, *78*, 1393–1407.
[14] D. Schröder, S. Shaik, H. Schwarz, *Acc. Chem. Res.* **2000**, *33*, 139–145.
[15] D. Usharani, D. Janardanan, C. Li, S. Shaik, *Acc. Chem. Res.* **2012**, *46*, 471–482.
[16] S. Shaik, H. Hirao, D. Kumar, *Acc. Chem. Res.* **2007**, *40*, 532–542.
[17] M. R. Bukowski, P. Comba, C. Limberg, M. Merz, L. Que Jr., T. Wistuba, *Angew. Chem. Int. Ed.* **2004**, *43*, 1283–1287.
[18] J. Bautz, M. Bukowski, M. Kerscher, A. Stubna, P. Comba, A. Lienke, E. Münck, L. Que Jr, *Angew. Chem. Int. Ed.* **2006**, *45*, 5681.
[19] J. Bautz, P. Comba, C. Lopez de Laorden, M. Menzel, G. Rajaraman, *Angew. Chem. Int. Ed.* **2007**, *46*, 8067.
[20] P. Comba, M. Maurer, P. Vadivelu, *Inorg. Chem.* **2009**, *48*, 10389–10396.
[21] P. Comba, S. Wunderlich, *Chem. Eur. J.* **2010**, *16*, 7293–7299.
[22] J. Madhavan, P. Comba, M. Maurer, P. Vadivelu, M. V. Venuvanalingham, *Dalton Trans. (Special Issue Computational Chemistry of Inorganic Systems)* **2011**, *40*, 11276–11281.
[23] P. Comba, G. Rajaraman, H. Rohwer, *Inorg. Chem.* **2007**, *46*, 3826–3838.
[24] P. Comba, M. Maurer, P. Vadivelu, *J. Phys. Chem. A* **2008**, *112*, 13028–13036.
[25] P. Comba, G. Rajaraman, *Inorg. Chem.* **2008**, *47*, 78.
[26] G. Mukherjee, C. V. Sastri, *Isr. J. Chem.* **2020**, *60*, 1–18.
[27] C. Bleiholder, H. Börzel, P. Comba, R. Ferrari, A. Heydt, M. Kerscher, S. Kuwata, G. Laurenczy, G. A. Lawrance, A. Lienke, B. Martin, M. Merz, B. Nuber, H. Pritzkow, *Inorg. Chem.* **2005**, *44*, 8145–8155.
[28] P. Comba, M. Kerscher, W. Schiek, *Prog. Inorg. Chem.* **2007**, *55*, 613–704.
[29] P. Comba, M. Kerscher, K. Rück, M. Starke, *Dalton Trans.* **2018**, *47*, 9202–9220.
[30] P. Comba, D. Faltermeier, S. Krieg, B. Martin, G. Rajaraman, *Dalton* **2020**, *49*, 2888–2894.
[31] P. Comba, S. Fukuzumi, H. Kotani, S. Wunderlich, *Angew. Chem. Int. Ed.* **2010**, *49*, 2622–2625.
[32] A. N. Biswas, M. Puri, K. K. Meier, W. N. Oloo, G. T. Rohde, E. L. Bominaar, E. Münck, L. Que Jr, *J. Am. Chem. Soc.* **2015**, *137*, 2428–2431.
[33] D. Wang, E. R. Farquhar, A. Stubna, E. Münck, L. Que Jr, *J. Am. Chem. Soc.* **2009**, *1*, 145–150.
[34] J. C. Price, E. W. Barr, L. M. Hoffart, C. Krebs, J. M. Bollinger Jr., *Biochem.* **2005**, *44*, 8138–8147.
[35] B. J. Brazeau, J. D. Lipscomb, *Biochem.* **2000**, *39*, 13503–13515.
[36] A. M. Valentine, S. S. Stahl, S. J. Lippard, *J. Am. Chem. Soc.* **1999**, *121*, 3876–3887.
[37] The first order rate of $[(L^1)Fe^{IV}=O(Cl)]^+$ with cyclohexane at −90 °C in EtCN is (2.0 ± 0.2) 10^{-1} s^{-1}, the second order rate is (7.55 ± 0.27) 10^2 $M^{-1}s^{-1}$ (see below), the second order rate of the second most reactive ferryl oxidant (a TPA derivative, TQA, with an $S=2$ ground state) with cyclohexane at −40 °C in MeCN is 3.7 10^{-1} $M^{-1}s^{-1}$,[32] the second order rate of an $Fe^{IV}_2(\mu\text{-}O)$ model complex (MeCN, 10 °C) is 8 10^{-2} $M^{-1}s^{-1}$.[33] The first order rate of the enzyme (TauD, H_2O, 5 °C) is

13 s^{-1},[34] the second order rate of methane monooxygenase (MMO–Q with an $Fe^{IV}_2(\mu\text{-}O_2)$ core) at 25 °C is 3–4 10^4 $M^{-1}s^{-1}$.[35,36] Note that, obviously, a direct comparison is difficult since the conditions of the experiments are strikingly different, and none of the experiments have been performed at controlled ionic strength, i.e. it is not possible to make scientifically valid direct comparisons. With this note of caution in mind, it seems to be appropriate to assume that the species discussed here with an $S=1$ ground state has a very similar rate, i.e. is at most 1 order of magnitude slower than the $S=2$ enzymes and approx. 4 orders of magnitude faster than the next fastest model system that has an $S=2$ ground state.

[38] Note that the relative concentrations in the various experiments are different for technical reasons, and this needs to be considered in the overall comparison and mechanistic interpretations (all reactions were performed in dry MeCN or dry EtCN under Ar and without addition of inert electrolytes): for MS experiments the concentration of $[(L^1)Fe^{II}Cl_2]$ was 10 μM, and 0.5-10 equiv. of ^{s}PhIO were added (ambient temperature, reaction time of approx. 1 h); (ii) for the kinetic experiments, the concentrations of $[(L^1)Fe^{II}Cl_2]$ were either 75 μM (decay of the precursor) or 2 mM (formation and decay of $[(L^1)Fe^{IV}=O(Cl)]^+$; (iii) for the bulk experiments, $[(L^1)Fe^{II}Cl_2]$ generally was 7 mM.

[39] M. Balamurugan, E. Suresh, M. Palaniandavar, *Dalton Trans.* **2016**, *45*, 11422–11436.

[40] A. J. Jasniewski, J. Que, *Chem. Rev.* **2018**, *118*, 2554–2592.

[41] S. Walleck, T. Glaser, *Isr. J. Chem.* **2020**, *60*, 1019–1031.

[42] J. H. Groß, *Mass Spectrometry*, Springer Heidelberg, Dordrecht, London, New York, **2004**.

[43] J. England, Y. Guo, E. R. Farquhar, V. G. Young Jr., E. Münck, L. Que Jr, *J. Am. Chem. Soc.* **2004**, *132*, 8635–8644.

[44] P. Comba, M. Kerscher, M. Merz, V. Müller, H. Pritzkow, R. Remenyi, W. Schiek, Y. Xiong, *Chem. Eur. J.* **2002**, *8*, 5750–5760.

[45] H. Börzel, P. Comba, C. Katsichtis, W. Kiefer, A. Lienke, V. Nagel, H. Pritzkow, *Chem. Eur. J.* **1999**, *5*, 1716–1721.

[46] P. Comba, S. Kuwata, G. Linti, M. Tarnai, H. Wadepohl, *Chem. Commun.* **2006**, 2074–2076.

[47] Note that, due to the weakly coordinating counter ions the doubly charged complex undergoes a charge reduction process in the ESI-MS experiment, leading to the formation of methanolate, which coordinates to the iron center. Since methanol is a widely used solvent for MS experiments, residual methanol is generally found in the measurement setup.

[48] A. Anastasi, P. Comba, J. McGrady, A. Lienke, H. Rohwer, *Inorg. Chem.* **2007**, *46*, 6420–6426.

[49] Because reaction rates depend on activities rather than concentrations, kinetics need to be measured at well-defined and constant ionic strength. However, for two reasons and as generally done in this field, this was neglected: Although more generally valid, these data would be difficult to compare with literature data on the formation and reactivity of other ferryl complexes (often measured in MeCN at millimolar concentrations of the iron(II) precursor and with excess oxidant and/or substrate, i.e. pseudo-first order conditions and similar to the experimental conditions used here). (ii) There are potential reactions of various electrolyte anions with the iron(II) precursor, the iron(IV) oxidant and iron(III) intermediates, including anation as well as redox processes (e.g. Cl^- is oxidized by the ferryl complexes reported here to hypochlorite, and this would be a further deactivation process of the ferryl oxidant, see Supporting Information, Figure S13).

[50] Note that the reactivity of $[(L^1)Fe^{IV}=O(Br)]^+$ has not yet been studied in detail, and the interpretation given assumes that the bromido complex follows the same pathways as the chlorido complex; this needs to be confirmed.

[51] O. Planas, M. Clemancey, J.-M. Latour, A. Company, M. Costas, *Chem. Commun.* **2014**, *50*, 10887–10890.

[52] Note that experiments to support the assignment of the fast reaction with cyclohexane as C–H activation, for example the measurement of kinetic isotope effects and reactions with other substrates are in progress.

[53] J. Kaizer, E. J. Klinker, N. Y. Oh, J. U. Rohde, W. J. Song, A. Stubna, J. Kim, E. Münck, W. Nam, L. Que, *J. Am. Chem. Soc.* **2004**, *126*, 472–473.

[54] M. S. Seo, N. H. Kim, K. B. Cho, J. E. So, S. K. Park, M. Clemancey, R. Garcia-Serres, J. M. Latour, S. Shaik, W. Nam, *Chem. Sci.* **2011**, *2*, 1039–1045.

[55] M. Atanasov, P. Comba, B. Martin, V. Müller, G. Rajaraman, H. Rohwer, S. Wunderlich, *J. Comb. Chem.* **2006**, *27*, 1263.

[56] C. Geng, S. Ye, F. Neese, *Angew. Chem. Int. Ed.* **2010**, *49*, 5717–5720.

[57] M. Swart, *Chem. Phys. Lett.* **2013**, *580*, 166–171.

[58] P. Verma, Z. Varga, J. E. M. N. Klein, C. J. Cramer, L. Que Jr, D. G. Truhlar, *Phys. Chem. Chem. Phys.* **2017**, *19*, 13049–13069.

[59] Q. M. Phung, M. Feldt, J. N. Harvey, K. Pierloot, *J. Chem. Theory Comput.* **2018**, *14*, 2446–2455.

[60] F. Vlahovic, M. Gruden, S. Stepanovic, M. Swart, *J. Quantum Chem.* **2020**, *120*, e26121.

[61] K.-B. Cho, Y.-M. Lee, Y. H. Kwon, S. Shaik, W. Nam, *J. Am. Chem. Soc.* **2012**, *134*, 20222–20225.

[62] M. Puri, A. N. Biswas, R. Fan, Y. Guo, L. Que, *J. Am. Chem. Soc.* **2016**, *138*, 2484–2487.

[63] K. B. Cho, H. Hirao, S. Shaik, W. Nam, *Chem. Soc. Rev.* **2016**, *45*, 1197–1210.

[64] M. R. Bukowski, P. Comba, A. Lienke, C. Limberg, C. Lopez de Laorden, R. Mas-Balleste, M. Merz, L. Que Jr., *Angew. Chem. Int. Ed.* **2006**, *45*, 3446.

[65] G. A. Russel, *J. Am. Chem. Soc.* **1957**, *79*, 3871.

[66] P. Comba, D. Faltermeier, B. Martin, *Z. Anorg. Allg. Chem. (Special Issue for H. W. Roesky)* **2020**, *646*, 1839–1845.

[67] H. Börzel, P. Comba, K. S. Hagen, M. Merz, Y. D. Lampeka, A. Lienke, G. Linti, H. Pritzkow, L. V. Tsymbal, *Inorg. Chim. Acta* **2002**, *337*, 407–419.

[68] B. V. Meprathu, J. D. Protasiewicz, ARKIVOC **2003**, 83–90.

[69] S. E. Gibson, N. Guillo, A. J. P. White, D. J. Williams, *J. Chem. Soc.-Perkin Trans.* **1996**, *1*, 2575–2581.

[70] D. Macikenas, E. Skrzypczak-Jankun, J. D. Protasiewicz, *J. Am. Chem. Soc.* **1999**, *121*, 7164–7165.

[71] P. Comba, L. Grimm, C. Orvig, K. Rück, H. Wadepohl, *Inorg. Chem.* **2016**, *55*, 12531–12543.

[72] U. Kuhl, W. Englberger, M. Haurand, U. Holzgrabe, *Arch. Pharm. Pharm. Med. Chem.* **2000**, *333*, 226–230.

[73] P. Comba, H. Rudolf, H. Wadepohl, *Dalton Trans.* **2015**, *44*, 2724–2736.

[74] A. D. Becke, *J. Chem. Phys. B* **1993**, *98*, 5648–5652.

[75] A. D. Becke, *J. Chem. Phys.* **1992**, *96*, 2155.

[76] A. D. Becke, *J. Chem. Phys.* **1992**, *97*, 9173–9177.

[77] P. Comba, A. Lienke, *Inorg. Chem.* **2001**, *40*, 5206–5209.

[78] P. Comba, B. Martin, A. Muruganantham, J. Straub, *Inorg. Chem.* **2012**, *51*, 9214–9225.

[79] P. Barman, A. K. Vardhaman, B. Martin, S. J. Wörner, C. V. Sastri, P. Comba, *Angew. Chem. Int. Ed.* **2015**, *54*, 2095–2099.

[80] W. R. Wadt, P. J. Hay, *J. Chem. Phys.* **1985**, *82*, 284–298.

[81] P. J. Hay, W. R. Wadt, *J. Chem. Phys.* **1985**, *82*, 270–283.

[82] W. J. Hehre, R. Ditchfield, J. A. Pople, *J. Chem. Phys.* **1972**, *56*, 2257.

[83] A. Schäfer, C. Huber, R. Ahlrichs, *J. Chem. Phys.* **1994**, *100*, 5829–5835.

[84] M. T. Cancès, B. Mennucci, J. Tomasi, *J. Chem. Phys.* **1997**, *107*, 3032–3041.

[85] M. Cossi, B. Barone, B. Mennucci, J. Tomasi, *Chem. Phys. Lett.* **1998**, *286*, 253–260.

[86] B. Mennucci, J. Tomasi, *J. Chem. Phys.* **1997**, *106*, 5151–5158.

[87] M. Cossi, G. Scalmani, N. Raga, V. Barone, *J. Chem. Phys.* **2002**, *117*, 43–54.

[88] F. Weinhold and C. R. Landis, *Valency and Bonding: A Natural Bond Orbital Donor Acceptor Perspective*, Cambridge, U. K., **2005**.

[89] A. E. Reed, L. A. Curtiss, F. Weinhold, *Chem. Rev.* **1988**, *88*, 899.

[90] M. J. Frisch, G. W. Trucks, H. B. Schlegel, G. E. Scuseria, M. A. Robb, J. R. Cheeseman, G. Scalmani, V. Barone, B. Mennucci, G. A. Petersson, H. Nakatsuji, M. Caricato, X. Li, H. P. Hratchian, A. F. Izmaylov, J. Bloino, G. Zheng, J. L. Sonnenberg, M. Hada, M. Ehara, K. Toyota, R. Fukuda, J. Hasegawa, M. Ishida, T. Nakajima, Y. Honda, O. Kitao, H. Nakai, T. Vreven, J. A. Montgomery Jr., J. E. Peralta, F. Ogliaro, M. Bearpark, J. J. Heyd, E. Brothers, K. N. Kudin, V. N. Staroverov, R. Kobayashi, J. Normand, K. Raghavachari, A. Rendell, J. C. Burant, S. Iyengar, J. Tomasi, M. Cossi, N. Rega, N. J. Millam, M. Klene, J. E. Knox, J. B. Cross, V. Bakken, C. Adamo, J. Jaramillo, R. Gomperts, R. E. Stratmann, O. Yazyev, A. J. Austin, R. Cammi, C. Pomelli, J. W. Ochterski, R. L. Martin, K. Morokuma, V. G. Zakrzewski, G. A. Voth, P. Salvador, J. J. Dannenberg, S. Dapprich, A. D. Daniels, O. Farkas, J. B. Foresman, J. V. Ortiz, J. Cioslowski and D. J. Fox, Gaussian, Inc., Wallingford CT, **2009**.

Manuscript received: March 23, 2021
Accepted manuscript online: June 14, 2021
Version of record online: July 5, 2021

